Technology maturity for the habitable-zone exoplanet imaging observatory (HabEx) concept

Rhonda Morgan, Keith Warfield, Gary Kuan, H. Phil P. Stahl, Bertrand Mennesson, et al.

Rhonda Morgan, Keith Warfield, Gary Kuan, H. Phil P. Stahl, Bertrand Mennesson, Bala Balasubramanian, Dimitri Mawet, Shouleh Nikzad, Joel Nissen, Stuart Shaklan, Eugene Serabyn, Karl Stapelfeldt, Steven Warwick, "Technology maturity for the habitable-zone exoplanet imaging observatory (HabEx) concept," Proc. SPIE 10698, Space Telescopes and Instrumentation 2018: Optical, Infrared, and Millimeter Wave, 106980S (6 July 2018); doi: 10.1117/12.2313845

SPIE.

Event: SPIE Astronomical Telescopes + Instrumentation, 2018, Austin, Texas, United States

Technology Maturity for the Habitable-zone Exoplanet Imaging Observatory (HabEx) Concept

Rhonda Morgan*[a], Keith Warfield[a], Gary Kuan[a], H. Phil Stahl[b], Bertrand Mennesson[a], Bala Balasubramaian[a], Dimitri Mawet[c], Shouleh Nikzad[a], Joel Nissen[a], Stuart Shaklan[a], Eugene Serabyn[a], Karl Stapelfeldt[a], Steve Warwick[d]

[a]Jet Propulsion Laboratory, California Institute of Technology, [b]NASA Marshall Space Flight Center, [c]California Institute of Technology, [d]Northrop Grumman

ABSTRACT

HabEx Architecture A is a 4m unobscured telescope mission concept optimized for direct imaging and spectroscopy of potentially habitable exoplanets, and also enables a wide range of general astrophysics science. The exoplanet detection and characterization drives the enabling core technologies. A hybrid starlight suppression approach of a starshade and coronagraph diversifies technology maturation risk. In this paper we assess these exoplanet-driven technologies, including elements of coronagraphs, starshades, mirrors, jitter mitigation, wavefront control, and detectors. By utilizing high technology readiness solutions where feasible, and identifying required technology development that can begin early, HabEx will be well positioned for assessment by the community in 2020 Astrophysics Decadal Survey.

Keywords: exoplanets, technology gaps, HabEx, detectors, coronagraph, starshade, deformable mirror

1. INTRODUCTION

Advances in technology over the last 10 years and ongoing development have enabled HabEx mission concept Architecture A to possibly reach Technology Readiness Level (TRL) 5 by 2026. The design strategy chose mature technologies and minimized risk. Table 1 summarizes the HabEx technology challenges, including the TRL expected by 2019 when the HabEx report is expected to be submitted to the Astrophysics Decadal Review Committee, and the TRL expected by 2022 when the Starshade to TRL 5 (S5) project is scheduled to complete.

The HabEx technology discussion covers current state of the art (SOA) as well as anticipated maturity path and dates, especially the milestone dates of 2019 and 2022. Many of the enabling technologies are at or expected to be at TRL 5 by 2019 and the remaining technologies are at TRL 4. Only one technology is currently at TRL 3 and is expected to mature to TRL 5 by 2022 as part of the Starshade to TRL 5 (S5) project.

Observatory science could be enhanced by extending the ultraviolet (UV) wavelength down to 100 nm if a compatible mirror coating is available. If such a coating is available, then delta-doped charge-coupled devices (CCDs) capable of operating in the ultraviolet could simplify UV instrument designs. If these technologies mature in time to be included, they would be worthwhile additions to the mission performance.

1.1 Note on the Starshade to TRL 5 (S5) Project

The starshade technology gaps and maturation plans were first identified in the NASA-commissioned, community-led, Exo-S study report (Seager et al. 2015). They were adopted by the NASA Exoplanet Exploration Program (ExEP) and tracked in the ExEP Technology Plan Appendix. In November 2016, the Starshade Readiness Working Group recommended to the NASA Astrophysics Director a plan to validate starshade technologies "that is both necessary and sufficient prior to building and flying" a starshade WFIRST Rendezvous mission. With the full concurrence of an independent Technical Advisory Committee, it was determined that "a ground-only development strategy exists to enable a starshade science flight mission" and "a prior flight technology demonstration is not required" (Blackwood 2016).

At the core of the S5 activity, "starshade shape accuracy and stability requirements are derived from a comprehensive error budget that will be verified by mechanical and optical performance models anchored to subscale ground tests." These performance models address the five technologies (Ziemer 2018). S5 matures the majority of the starshade gaps for the HabEx mission concept as well.

*rhonda.morgan@jpl.nasa.gov; phone 1 818-393-2321

Space Telescopes and Instrumentation 2018: Optical, Infrared, and Millimeter Wave, edited by Makenzie Lystrup, Howard A. MacEwen, Giovanni G. Fazio, Proc. of SPIE Vol. 10698, 106980S
 · doi: 10.1117/12.2313845

Table 1. HabEx 4-m Hybrid Architecture Technology Gap List

Title	Description	State of the Art	Capability Needed	Expected TRL	
				2019	2022
Technology Challenges for the 4-Meter Architecture					
Starshade Petal Deployment Position Accuracy	Deploy and maintain petal position accuracy in L2 environment	• Petal deployment tolerance (≤0.15 mm) verified with multiple deployments of 12 m flight-like perimeter truss and no optical shield • No environmental testing	• Petal radial deployment accuracy on 40 m perimeter truss: ±500 μm (3σ) bias • Position stability in operational environment: ±1.5 mm (3σ) random	3	4
Technologies Approaching TRL 5					
Starshade Petal Shape and Stability	Starshade petal shape maintained after deployment, thermal at L2	• Manufacturing tolerance (≤100 μm) verified with low fidelity 6 m prototype • No environmental tests • Petal deployment tests conducted on prototype petals to demonstrate rib actuation • No deployed petal shape measurements	• Petal shape manufacture: ±170 μm (3σ) • Postdeployment 16 m petal shape demonstrated to ≤ ±156 μm (3σ) • Stability (thermal): disk to petal strain ≤30 ppm, 1–5 cycle/petal width ≤ 20 ppm	4	5
Large Mirror Fabrication	Large monolith mirror that meets tight surface figure error and thermal control requirements at visible wavelengths	• Schott demonstrated CNC lightweighting to pocket depth of 340 mm, 4 mm rib thickness (E-ELT M5) • State of the practice (SOP) lightweighting has yielded large mirrors of aerial density 70 kg/m^2 • Zerodur can achieve 5 parts per billion/K CTE homogeneity • Wavefront stability: ~10 nm rms	• Current SOA lightweighting is sufficient to meet SLS launch capabilities • Wavefront thermal stability of ~1 nm rms between consecutive low-order wavefront updates which are 100 s of seconds apart • First mode ≥ 60 Hz	4	4
Large Mirror Coating	Mirror coating with high spatial uniformity over the visible spectrum	• IUE, HST, and GALEX used MgF_2 on Al to obtain >70% reflectivity from 115 nm to 2,500 nm • Reflectance non-uniformity <0.5% of protected Ag on 2.5 m TPF Technology Demonstration Mirror • Operational life: > 28 years on HST	• Reflectivity from 115–1,800 nm • Reflectance uniformity <1% over 450–1,000 nm • Operational life >10 years	4	4
Coronagraph Architecture	Suppress starlight by a factor of ≤ 1E-10 at visible and NIR wavelengths	• Hybrid Lyot: 6×10^{-10} raw contrast at 10% bandwidth across angles of 3–16 λ/D demonstrated with a linear mask and an unobscured pupil in a static vacuum lab environment • Vector vortex charge 4: 5×10^{-10} raw contrast monochromatic across angles of 2–7 λ/D demonstrated with an unobscured pupil in a static vacuum lab environment	• Raw contrast of ≤ 1×10^{-10} • Raw contrast stability of ≤ 2×10^{-11} • IWA ≤ 2.4 λ/D • Coronagraph throughput ≥10% • Bandwidth ≥20%	4	5
LOWFS	Sensing and control of low-order wavefront drift	• <0.2 mas rms per axis LoS residual error demonstrated in lab with a fast-steering mirror attenuating a 14 mas LoS jitter and reaction wheel inputs; 12 pm rms sensitivity of low order modes (WFIRST) • WFE stability of 25 nm/orbit in low Earth orbit-higher low-order modes sensed to 10–100 nm WFE rms on ground-based telescopes	• LoS error < 0.5 mas rms • WF stability:≤~100 pm rms over 1 second for vector vortex • WFE <0.76 nm rms	4	5

Title	Description	State of the Art	Capability Needed	Expected TRL	
				2019	2022
Deformable Mirrors	Flight-qualified large-format deformable mirror	• Micro-electromechanical DMs available up to 64 × 64 actuators with 6 nm RMS flattened WFE • Smaller DMs supported coronagraph demonstrations of 2×10^{-7} raw contrast at 10% bandwidth in a static test	• 64×64 actuators. • Enable coronagraph raw contrasts of $\leq1\times10^{-10}$ at ~20% bandwidth and raw contrast stability $\leq2\times10^{-11}$	4	5
Starshade Edge Scattering	Limit edge-scattered sunlight and diffracted starlight with optical petal edges	• Machined graphite edges solar glint flux: 25 visual magnitudes in two main lobes • Metal edges meet all specs but in-plane shape tolerance	• Petal edge in-plane shape: 40 µm • Solar glint: 28 visual magnitudes in two main lobes	4	5
Technologies at TRL 5 or Higher					
Starshade Modeling and Performance	Validate at flight-like Fresnel numbers the equations that predict the contrasts	• 6×10^{-6} suppression in pupil at F1.0 ~15 • 4.8×10^{-8} suppression in pupil, 5×10^{-10} contrast demonstrated at F1.0 ~27 (monochromatic)	• Experimentally validated models with total starlight suppression ≤ 1E–8 in scaled flight-like geometry, with F1.0 between 5 and 40 across a broadband optical bandpass. Validated models are traceable to 1E-10 contrast system performance in space	5	5
Starshade Lateral Formation Sensing	Lateral formation flying sensing to keep telescope in starshade's dark shadow	• Simulations have shown centroid star positions to ≤1/100th pixel with ample flux to support control loop • Sensing demonstration of lateral control has not yet been performed	• Demonstrate sensing lateral errors ≤0.20 m accuracy at scaled flight separations (≤1 mas bearing angle) • Control algorithms demonstrated with scaled lateral control errors corresponding to ≤1 m	5	5
Microthrusters	Jitter is mitigated by using microthrusters instead of reaction wheels during exoplanet observations	• Colloidal microthrusters 5–30 µN thrust with a resolution of ≤ 0.1 µN , 100 days on-orbit on LISA Pathfinder • Cold gas micronewton thrusters flown on Gaia (TRL 9), 0.1 µN resolution, 1 mN max thrust, 4 years of on-orbit operation	• Thrust capability: 0.35 mN • Operating life: 5 years	5	5
Laser Metrology	Sensing for control of rigid body alignment of telescope front-end optics	• Thermally stabilized Planar Lightwave Circuit fully tested • Nd:YAG ring laser and modulator flown on LISA Pathfinder • Phase meters flown on LISA Pathfinder	• Sense at 1 kHz bandwidth • Uncorrelated per gauge error of 0.1 nm	5	5

Delta-Doped Visible Electron Multiplying CCDs	Low-noise visible detectors for exoplanet characterization via integral field spectrograph	• 1k×1k EMCCD detectors (WFIRST)
		  ○ dark current of 7×10^{-4} e-/px/s
		  ○ CIC of 2.3×10^{-3} e-/px/fram
		  ○ read noise ~0 e- rms (in EM mode)
		  ○ Irradiated to equivalent of 6 year flux at L2
		• 4k × 4k EMCCD fabricated with reasonable performance
			• 450–1,000 nm response;
			• dark current < 10^{-4} e-/px/s
			• CIC < 3×10^{-3} e-/px/fram;
			• effective read noise <0.1e- rms;
			• tolerant to a space radiation environment over mission lifetime at L2
			• 4k × 4k format
				5	5

Title	Description	State of the Art	Capability Needed	Expected TRL	
				2019	2022
Linear Mode Avalanche Photodiode Sensors	Near infrared wavelength (900 nm to 2.5 µm), extremely low noise detectors for exo-Earth IFS	• HgCdTe photodiode arrays have read noise <~2 e- rms with multiple non-destructive reads; dark current <0.001 e-/s/pix; very radiation tolerant (JWST) • HgCdTe APDs have dark current ~ 10–20 e-/s/pix, read noise <<1 e- rms, and < 1k × 1k format • eAPD have 0.0015 e-/pix/s dark current, <1 to 0.1 e rms readout noise (SAPHIRA)	• Read noise <<1 e- rms • Dark current <0.002 e-/pix/s • In a space radiation environment over mission lifetime	5	5
UV Microchannel Plate (MCP) Detectors	Low noise detectors for general astrophysics as low as 115 nm	• MCPs: QE 44% 115-180 nm with alkalai photocathode, 20% with GaN; dark current ≤0.1-1 counts/cm^2/s with ALD borosilicate plates	• Dark current <0.001 e-/pix/s [173.6 counts/cm^2/s], in a space radiation environment over mission lifetime, • high QE for 115–350 nm wavelengths	5	5
Delta-Doped UV Electron Multiplying CCDs	Low noise detectors for general astrophysics as low as 100 nm	• Delta doped EMCCDs: Same noise performance as visible with addition of high UV QE ~ 60–80% in 100–350 nm, dark current of 3×10^{-5} e-/pix/s beginning of life. 4k × 4k EMCCD fabricated with promising performance and mitigation of cosmic ray. Dark current <0.001 e-/pix/s, in a space radiation environment over mission lifetime, ≥4k × 4k format for spectrograph, high QE for 100–350 nm wavelengths	• Dark current <0.001 e-/pix/s, in a space radiation environment over mission lifetime, • ≥4k × 4k format for spectrograph, • high QE for 100–350 nm wavelengths	5	5
Enhancing					
Far-UV Enhanced Coatings	General astrophysics imaging as low as 100 nm	• For a 100 nm cutoff, Al + LiF + AlF3 has been demonstrated at the lab proof-of-concept level with test coupons achieving reflectivities of 80%+ for >200 nm and 60% at 100 nm and 3-year lab environment stability	• Reflectivity from 300–1,800 nm: > 90% • Reflectivity from 115–300 nm: > 80% • Reflectivity below 115 nm: > 50% • Operational life: > 10 years	3	3

2. TECHNOLOGY CHALLENGES FOR THE 4 METER ARCHITECTURE

The primary HabEx technology challenge is starshade petal deployment position accuracy because maturation beyond S5 may be required. HabEx will advance to TRL 4 through the S5 task, but a larger test unit would be needed to bring HabEx to TRL 5. HabEx would leverage the S5 technology development activity and modify the S5 plan for a larger structure. HabEx is also assessing reducing the size of the baseline starshade. If the starshade can be reduced significantly without loss to science, then this one remaining technology gap may be completed to TRL 5 through the S5 effort.

2.1 Starshade Petal Deployment Position Accuracy

The starshade must have the ability to stow, launch, and deploy the petals and inner disk to within the deployment tolerances budgeted to meet the shape, and ultimately, the contrast requirements. The optical shields within both the petals and the inner disk must fully deploy intact with no damage.

For the S5 activity a half-scale flight-like structure will be built to demonstrate deployment tolerances. In April 2018, the Starshade Mechanical Architecture Trade Review evaluated NGAS deployment architecture and the wrapped (JPL) deployment architecture, which met design requirements with generous margin. The JPL wrapped petal design is the HabEx baseline architecture and allows for co-launch of the starshade and telescope in a single SLS Block 1B fairing.

As concluded by Shaklan et al. (2017), "for a given level of performance, the physical tolerances on a starshade scale roughly linearly with starshade size." The S5/WFIRST Rendezvous baseline reference starshade is 26 meters in diameter with a 10-meter diameter central disk and 8 m long petals, and S5 is likely to build at half-scale: a 5-meter diameter central disk with 4-meter petals. The HabEx starshade is 72 m diameter with a 40 m diameter central disk and 16 m long petals, a factor of 4 larger in scale than the S5 demonstrator, which would not be sufficient to advance the HabEx petal position and accuracy technology readiness. HabEx would need to plan beyond S5 for a demonstrator with 20-meter diameter perimeter truss and 8-meter petals.

HabEx is currently studying alternative starshade designs of smaller diameter which could allow the S5 development plan to bring petal deployment position accuracy for HabEx to TRL 5.

3. TECHNOLOGIES APPROACHING TRL 5

A number of key technologies needed for HabEx are currently at TRL 4 (large optics, mirror coatings, and coronagraph architecture) or are expected to be at TRL 4 by the release of the HabEx final report (low order wavefront sensing and control [LOWFS], starshade petal and starshade modeling). For most of these technologies, advancement to TRL 5 is expected by the end of FY2022. The exceptions are large mirror and mirror coating technology gaps, which are slowed from advancing to TRL 5 by the need for a prototype mirror. Development of a 4-meter mirror and construction of a suitable coating chamber will cost more than $50M, which is a significant commitment toward the large monolithic telescope architecture and likely to occur only with prioritization of a monolithic concept by the Decadal Survey.

This section discusses these approaching technologies, their current performance and their paths forward to TRL 5.

3.1 Starshade Petal Shape and Stability

The starshade must be able to deploy petals to the proper shape as well as maintain the shape during any given observation. The shape stability is dependent on the orientation of the starshade with respect to the Sun given the variation of temperatures across the passively temperature controlled structure.

This technology will require a half-scale, 8 meter, petal structure to bring it up to TRL 5. S5 is planning to build an 4m long petal with the width of a 8 m petal as part of its TRL 5 demonstration. This demonstration will also apply to HabEx as a half scale test article. As such, HabEx petal technology will advance with the S5 technology task. In the current S5 plan, the petal will reach TRL 4 in 2019 and TRL5 in 2022.

3.2 Large Aperture Monolithic Primary Mirror

HabEx selected a 4-m monolithic mirror design that is TRL 4. Two critical choices enable the design: the Space Launch System (SLS) allows for generous mirror mass so that SOA mirror lightweighting is sufficient, and replacing reaction wheels with microthrusters for pointing control during observations reduces jitter disturbances sufficiently to allow the use of an open-back Zerodur® design. In assessing the TRL of a large aperture monolith mirror, we consider the material, thermal stability, mechanical stability, and manufacturability.

As a material, Zerodur is TRL 9. Over 30 Zerodur mirror systems have flown in space; the largest in the visible band are the 0.8 m, 73% lightweighted mirrors on the meteosats; Chandra's cylindrical mirrors are also Zerodur, with the largest having a surface area of 1 m × 3 m. Zerodur coefficient of thermal expansion (CTE) is an excellent match to carbon-fiber metering structure material and can be 'tuned' to provide zero-CTE over a range of operational temperatures. Introduced in 2012, Zerodur Special achieves CTE homogeneity of 10 ppb/K and Zerodur Extreme achieves 7 ppb/K, and homogeneity of 1–5 ppb/K has been shown through thickness (Jedamzik and Westerhoff 2017). A CTE homogeneity of 10 ppb/K allow for wavefront thermal stability of ~1 nm rms between consecutive low-order wavefront updates which are 100s of seconds apart.

The ability to manufacture mirror blanks as large as 4 m has been demonstrated by Schott. Schott routinely makes 4.2 m diameter × 42 cm thick mirror blanks. A recent example is the Daniel K. Inouye (DKI) Advanced Solar Telescope mirror (Oh 2016). In addition, Schott regularly manufactures 2 m × 40 cm lightweight ultra-stiff structures from Zerodur® with ultra-CTE homogeneity for its lithography bench product line (Westerhoff and Werner 2017).

The mechanical stability required by using microthrusters is a ~60Hz first mode. Multiple designs are low mass and have first mode >60 Hz. Schott published a 4 m open-back point design that has a ~80 Hz first mode and a 718 kg mass (Hull et al. 2013). The best performing 4 m design came from United Technology Aerospace Systems (UTAS); it has a

first mode of 120 Hz while mounted on its bipod supports, and only weighs 1,200 kg. For the HabEx interim report, a 64 Hz first-mode, 1,356kg Marshall Space Flight Center (MSFC) design was adopted, though the UTAS design will be evaluated going forward.

For manufacturability of the surface error, UTAS has demonstrated the ability to fabricate mirrors with power spectral density appropriate for coronagraphy: total surface figures errors of <6 nm rms; mid-spatial-frequency error of <2 nm rms; and surface roughness of <1 nm rms. On Chandra, UTAS produced Zerodur mirror surfaces with a roughness of 0.2 nm rms. The keys to this level of precision include tribology, slurry concentrations, pressures, speeds, linkages to polishing tools, polishing environments, etc. These factors are understood by a handful of suppliers in the United States and Europe. Also key to this level of precision is the mirror's mechanical stiffness, both globally and locally. Polishing methods require accurate positional knowledge of mirror stiffness.

Figure 1. Baseline 4 m × 40 cm thick flat-back open-back isogrid core Zerodur mirror.

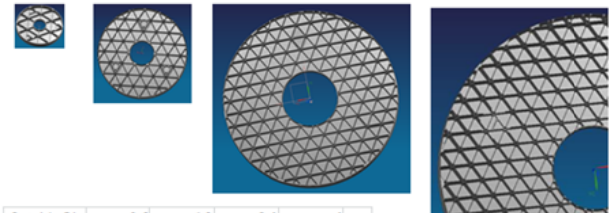

Outside Dia	0.6	1.2	2.4	4 m	
ROC	1.548	3.1	6.192	10.33	m
f/#	1.29	1.29	1.29	1.29	
Center Hole	0.160	0.320	0.750	1.080	m
Thickness	0.07	0.125	0.25	0.335	m
Mass	7.6	45	228	718	kg
fo	419	213	115	~80	Hz

Figure 2. Results of analysis of 0.6, 1.2, 2.4, and 4 m lightweight Zerodur mirror substrates by the SCHOTT process. Masses represented are consistent with most present and anticipated OTAs for spaceborne missions. Each case was constrained to satisfy launch load with strength margin, and launch locks are assumed for the 4 m case. Credit: Schott

A mirror system's self-weight deflection (i.e., gravity sag) and the accuracy to which it can be removed from a one gravity (1-G) measurement is a critical limitation for producing a zero gravity (0-G) mirror. The challenge is that the magnitude of gravity sag grows larger as mirror stiffness decreases. As gravity sag grows, so does the associated back-out error.

Any design of a 4 m mirror assembly must consider metrology capabilities to guide the optical surface finishing and demonstrate zero gravity surface figure. Specific items of attention must include surface figure and slope errors anticipated at different stages of manufacturing and under gravity load. Optical metrology accuracy, dynamic range, and spatial resolution are critical.

UTAS has TRL 9 experience designing and manufacturing 0-G mirrors as large as 2.5 m and ground-based mirrors as large as 4 m. The gravity flip metrology method allows empirical determination of gravity deformation in order to meet 0-G surface figure requirements without FEA-derived gravity compensation. Their method is self-verifiable by comparing results from different gravity flip orientations. UTAS has demonstrated TRL 9 ability to back-out gravity sag errors in mirrors as large as 2.5 m to an accuracy of less than 3 nm rms, typically limited by metrology uncertainty. Actuators on the back of the primary mirror could be considered to reduce risk with gravity sag back out.

3.3 Large Mirror Coating and Uniformity

All HabEx instruments are affected by the telescope mirror coating performance and must be considered when defining the mirror reflective properties. Telescope mirror coatings for the HabEx mission require:

- Spectral coverage with high throughput from 115 to 1,800 nm
- Uniformity of reflectivity–both amplitude and phase—of ≥99% over the full aperture are critical to achieve coronagraph contrast in the 10^{-10} level

- Consistent reflective properties for at least 10 years. Since HabEx is serviceable but cannot replace its mirrors, a coating that can last 20 or 30 years is highly desirable

This section describes both the high-heritage baseline coating and better-UV-performing alternatives that could be considered if they are technologically mature at the time of the future mission.

The current state-of-the-art for space telescope mirror coatings is summarized in **Table 2**. HabEx selected a Hubble Space Telescope (HST) like coating: an aluminum reflecting surface with a magnesium-fluoride protective overcoat. The materials and processes have been flight-proven by HST over the last 27 years and are at TRL 9. Silver and gold coatings do not meet the spectral range needed by HabEx, and though the lithium-fluoride overcoat used on the Far Ultraviolet Spectroscopic Explorer (FUSE) went below 100 nm in spectral coverage, the coating had degradation issues during the FUSE mission. Work to develop a stable LiF protected aluminum coating for spectral coverage below 115 nm continues. Should one be developed in time for a future HabEx mission, the improved coating would offer a significant enhancement to the current ultraviolet science case.

Table 2. State-of-the-art coatings for large aperture space telescope primary mirrors.

	HST	Kepler	JWST	FUSE
PM Size	2.4 m monolith	1.4 m monolith; 950 mm entrance aperture	18 hexagonal Be mirror segments (~1.52-m wide) with total collecting area of 25 sq m	Four mirrors of 38.7×35.2 cm each
Spectral Range	115–2,500 nm	300–1,200 nm	700 nm to 20 μm	90.5–118.7 nm
Operational Lifetime	>27 years	> 9 years	10 years max (Design Life)	8 years (had significant Al coating degradation)
Coating	Protected Al (MgF2 on Al)	Protected Ag (multilayer on Ag)	Protected Au	LiF on Al on 2 mirrors and SiC on other 2
Uniformity		<30 nm PV; Reflectivity variation <2%	<1% thickness variation among the 18 segments. <10 nm pv; Reflectance variation <0.5% in the IR	

3.4 Baseline Al+MgF2 Coating

Aluminum mirrors overcoated with MgF_2 have been used on space telescopes since the 1970s. Most notable is the mirror coating for the long-operating HST observatory. **Figure 3** shows a model of reflectance performance of a HST-like mirror coating in comparison with ideal Al with no overcoat. The coating on HST provides high reflectivity at wavelengths greater than ~120 nm. Below 115 nm, the reflectivity drops sharply to less than 20% due to the absorption edge of MgF_2. This level of performance is sufficient to meet HabEx baseline requirements.

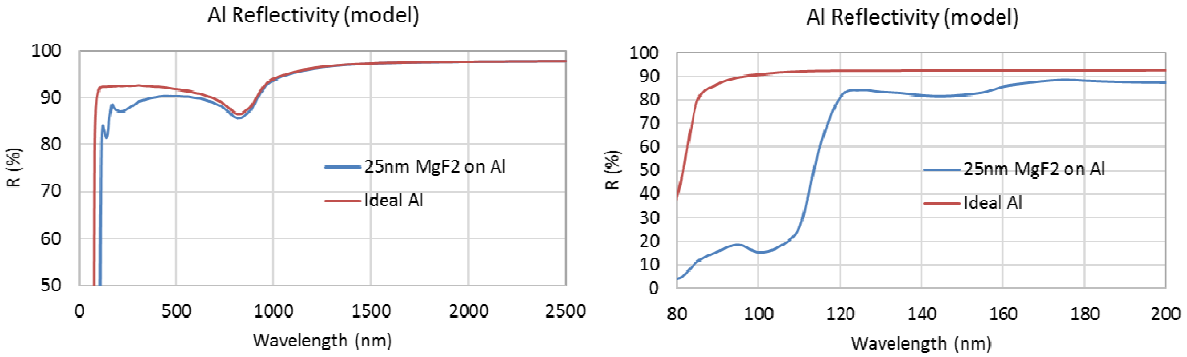

Figure 3. Aluminum reflectivity with and without a protective layer of MgF_2 (**HST-like model prediction**); the spikes and dips between 90 and 200 nm are a consequence of interference effects and absorption due to the protective layer and depends critically on the optical constants of the material, which depend on the coating process. The dip at ~830 nm is due to the native absorption property of Al.

Uniformity of the 4 m mirror coating is the primary coating issue for HabEx. Coating uniformity—specifically reflectivity phase and amplitude—is mainly a result of the coating process controls relevant to the specific chamber geometry. As such, engineering development is needed to build a sufficiently large chamber for the 4 m primary, and to optimize manufacturing processes to ensure a coating with less than 1% variability, as desired for HabEx.

The Kepler 1.4 m primary mirror has a protected silver coating generated using ion assisted deposition with a moving source, resulting in a thickness uniformity of about 30 nm peak-to-valley with about 2.5% reflectivity variation (Sheikh, Connell, and Dummer 2008). Better uniformity has been achieved on JWST. The JWST gold mirrors showed <10 nm peak-to-valley thickness non-uniformity with <0.5% reflectance non-uniformity in the infrared (IR) among its 18 hexagonal segments (Lightsey et al. 2012).

In 2004, Kodak (now Harris Corp, Rochester) demonstrated reflectivity variability of less than 0.5% for a high reflectivity protected silver coating over a 2.5 m diameter optic as part of the Terrestrial Planet Finder Technology Demonstration Mirror project (Cohen and Hull 2004).

These historical examples of large space mirrors with highly uniform protected metal coatings are subscale manufacturing demonstrations for a future 4 m HabEx mirror with an HST-like Al+MgF2 coating.

3.5 Far-UV Enhanced Coatings

Extending the coating performance down to ~100 nm in the far-UV (FUV) requires technology development. At present, some of the coatings capable of this spectral range are at ~TRL 3. Significant research and development (R&D) work is underway at JPL and Goddard Space Flight Center (GSFC) to accomplish FUV spectral coverage combined with long-term stability (Fleming et al 2017).

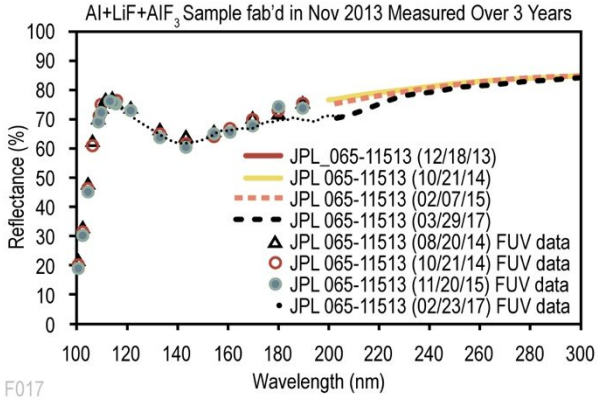

Figure 4. AlF^3 overcoat prevents LiF moisture degradation in lab environment (Balasubramanian et al 2017)

Some of the more promising candidates are new lithium-fluoride evaporation techniques and adding a second thin coating layer of aluminum-fluoride to protect the lithium-fluoride layer. Work at GSFC has explored evaporation of LiF at elevated substrate temperatures, which has been shown to improve performance and environmental stability over legacy LiF coatings such as those used on the FUSE mission. Although improved, these coatings still exhibit degradation of reflectance in moderate humidity storage conditions. This has motivated JPL research into a stacked approach where the GSFC LiF coating is itself protected by a second layer of AlF_3.

Early lifetime stability tests of the Al+LiF+AlF_3 are encouraging. Samples have been tested for reflectivity changes over a 3-year period. The samples were stored in normal laboratory conditions with relative humidity ranging from 20 to 50% at nominally 68°F. Measured performance is shown in **Figure 4** (Pham and Neff 2016), and (Balasubramanian et al. 2015, 2017).

Extending the spectral range of the HabEx telescope optics down to 100 nm is not in the current baseline design due to the technological maturation needed. Should continued investment in this technology result in a demonstrably stable coating able to meet uniformity requirements, then a future HabEx mission could elect to use such a coating in place of the current baseline HST-like coating.

3.6 Coronagraph Architecture

Tremendous progress in coronagraph performance has been made over the last decade. Through the efforts on the WFIRST technology demonstration coronagraph and several strategic technology investments by the NASA Exoplanet

Exploration Program, direct imaging contrast performance is nearing the levels required to detect Earth-sized planets in the habitable zone of nearby stars.

This section covers the SOA for the two coronagraph architectures in consideration by HabEx—the vector vortex coronagraph (VVC) and the hybrid Lyot coronagraph (HLC)—and the work needed to advance these technologies to TRL 5 with respect to HabEx requirements.

3.7 VVC and HLC Architectures

The current HabEx design uses the VVC as the baseline design and the HLC as a backup option. The block diagram in **Figure 5** identifies the major coronagraph elements common to both the VVC and the HLC: a fast steering mirror (FSM) to control pointing and mitigate jitter; two 64×64 deformable mirrors (DMs) to correct wavefront error (WFE); and a LOWFS to detect WFE. These architectures have nearly the same optical layout so they are of similar size and footprint, and could be exchanged even in a fairly advanced design with minimal impact, adding flexibility to any future mission development.

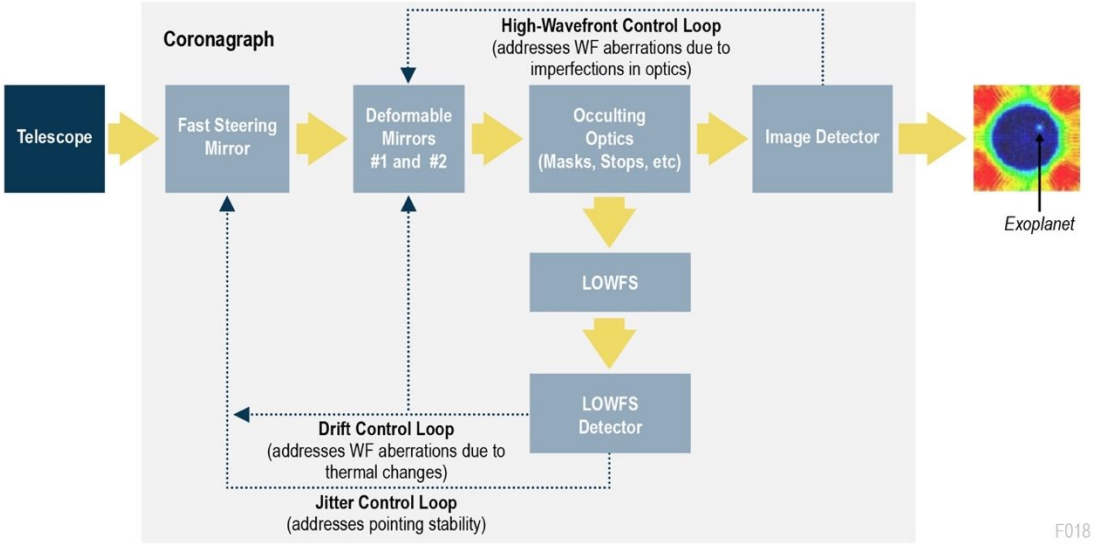

Figure 5. Coronagraph control loop block diagram

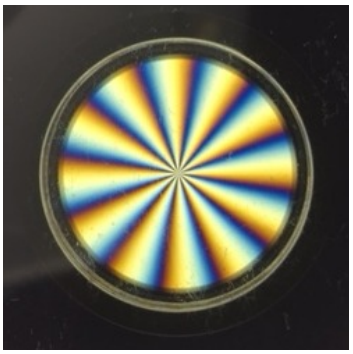

Figure 6. A charge 6 liquid crystal polymer vector vortex mask as seen through crossed polarizers. Credit: E. Sarabyn

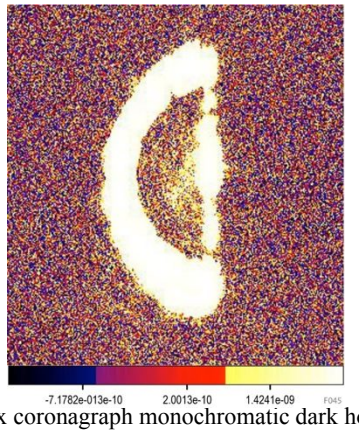

Figure 7. A vortex coronagraph monochromatic dark hole at the 5×10^{-10} level covering 2 to 7 λ/D (Serabyn et al. 2013).

The vortex coronagraph uses a focal-plane phase mask (**Figure 6**) to redirect the on-axis starlight to the outside of a subsequent pupil image, where it is blocked. The vortex phase pattern consists of an azimuthal phase ramp that reaches an even multiple of 2π radians in one circuit about the center of the mask. The very center of the vortex mask is usually

covered by a small opaque spot, to mask defects near the phase pattern's central singularity where the desired spatial orientation gradient is too large.

The HLC mask uses a partially opaque spot to block the majority of the target star light and an overlaid phase modulation pattern provided by an optimized dielectric layer. The HLC design includes optimized DM shapes that help make the coronagraph achromatic and mitigate sensitivity to low-order aberrations. In the HabEx evaluation, both the VVC and the HLC masks are slightly tilted and their central obscurations are reflective, sending incident starlight into the coronagraph's fine guidance sensor (FGS) and LOWFS.

3.8 State of the Art

The HLC has demonstrated the deepest starlight suppression to date (6×10^{-10} over 10% bandwidth from 3 to 16 λ/D) and is one of the two baseline coronagraphs of the WFIRST CGI (Trauger et al. 2015). While this is close to the HabEx requirement (1×10^{-10} contrast over a 20% bandwidth with an inner working angle at 2.4 λ/D), there is still work needed.

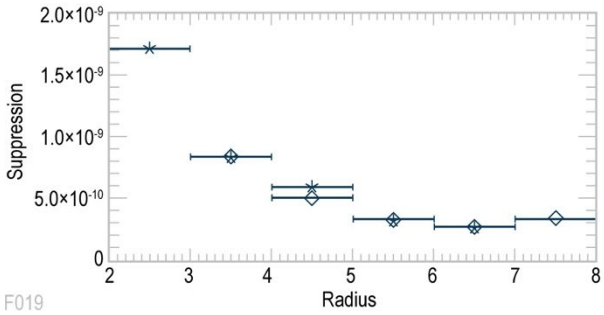

Figure 8. Cross-cuts through vortex dark holes of 2 to 7 λ/D (asterisks) and 3 to 8 λ/D (diamonds).

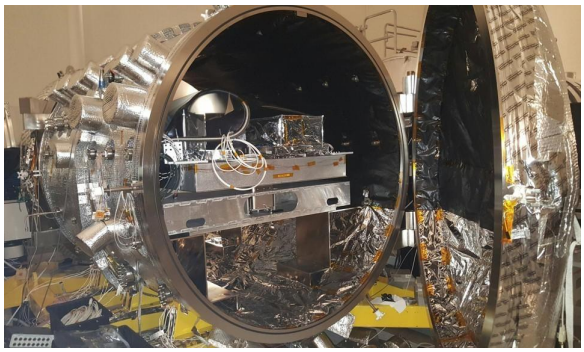

Figure 9. WFIRST CGI testbed.

In the first vortex-related Technology Demonstration for Exoplanet Mission (TDEM), carried out in the original high-contrast imaging testbed (HCIT) chamber, monochromatic contrasts of 5×10^{-10} were demonstrated (Serabyn et al. 2013) for dark holes extending both from 3 to 8 λ/D, and from 2 to 7 λ/D (**Figure 7**), demonstrating very good performance all the way into 2 λ/D (**Figure 8**). Since then, the goal has shifted to broadband performance. For broadband testing under a second TDEM, a new HCIT at JPL is being used. As a result, both the chamber and the vortices are being improved in tandem. Even so, contrasts for 10% bandwidths quickly reached the level of a few 10^{-8} of total leakage, which currently is dominated by a fairly uniform incoherent background, with the coherent contribution being a little above the 10^{-9} level. These tests resumed in May 2018.

3.9 Maturing the Technology

The HabEx coronagraph architecture follows the same development path as the one successfully completed by the WFIRST CGI (CGI testbed shown in **Figure 9**). First, the coronagraph undergoes a narrow-band static contrast test, then a broadband static test, and finally a broadband dynamic test. All testing will be carried out in the NASA HCIT. Both the VVC and the HLC will undergo the full development testing process. This approach provides alternatives should one of the coronagraphs not clear a development test.

The initial narrow-band test is necessary to demonstrate that each coronagraph is capable of reaching the required 10^{-10} raw contrast level. While the contrast level is more demanding than WFIRST, HabEx benefits from an aperture without obscurations. Coronagraph optics should be in a flight-like layout and include two 64×64 DMs. The testing should be carried out at about 500 nm, under vacuum, in a static environment. The test should be repeated with DM resets between each test to demonstrate consistency of performance.

The broadband test demonstrates that the coronagraphs can operate without significant chromatic problems. The test is conducted with a 20% band centered at 500 nm, in a static environment. To address chromatic issues, wavefront control is required. A control loop between the imaging detector and the DMs must be added at this point in the development. Data from the test can be used for post-processing algorithm development and optimizing wavefront control algorithms.

Finally, the HabEx coronagraphs must demonstrate broadband contrast under flight-like environmental conditions. To achieve this, an FSM and a LOWFS system are added to the testbed. LOWFS control loops correct for drift and jitter

using the FSM and the DMs. Again, the test is conducted in a 20% band centered at 500 nm and is repeated several times to demonstrate the consistency of the results. Once successfully completed, the coronagraphs will be at TRL 5.

One last note: the HabEx coronagraph is significantly larger than the WFIRST CGI, so an evaluation of the HCIT facilities must be conducted ahead of this technology development effort. Some facility upgrades may be necessary to complete the HabEx coronagraph testing program.

3.10 LOWFS and Control

The coronagraph LOWFS uses the rejected starlight from the coronagraph to sense the low order WFE, which includes line of sight (LOS) pointing error and thermal-induced low order wavefront drift. The LOWFS module consists of four elements fed by light reflecting off the coronagraph mask for both the HLC and the VVC.

The LOWFS sensor is a Zernike wavefront sensor (ZWFS) similar to the WFIRST CGI's LOWFS. The ZWFS is based on the Zernike phase contrasting principle where a small (~1–2 λ/D) phase dimple with phase difference of ~λ/2 is placed at center of the rejected starlight point spread function (PSF). The modulated PSF light is then collimated and forms a pupil image at the LOWFS camera. The interferences between the light passing inside and outside the phase dimple convert the wavefront phase error into the measurable intensity variations in the pupil image on the LOWFS camera. The spatial sampling of the pupil image on the LOWFS camera depends on the spatial frequency of WFE to be sensed. There is a design trade between number of sensed modes, photons per pixel, and the LOWFS camera frame rate. To improve the signal-to-noise ratio, the LOWFS uses broadband (>20%) light. The LOWFS camera is running at high temporal frequency (~1 KHz frame rate) in order to sense the fast LOS jitter.

The LOWFS-sensed tip-tilt errors are used to control the FSM for LOS disturbances correction. Similar to WFIRST CGI, the FSM LOS control loops contain a feedback loop to correct the telescope's LOS drift and a feedforward loop to suppress LOS jitter. The LOWFS sensed low order wavefront errors beyond tip-tilt will be corrected using one of the DMs.

ZWFS-based LOWFS has been developed, designed, and testbed demonstrated for WFIRST CGI at JPL's LOWFS testbed and occulting mask coronagraph (OMC) dynamic testbed, which has two coronagraph modes: hybrid Lyot coronagraph and shaped pupil coronagraph (SPC). Testbed results have shown that ZWFS is very sensitive, capable of sensing LOS less than 0.2 milliarcsec and low-order WFE as small as 12 picometer (rms). Recent OMC dynamic test results have demonstrated that with LOWFS FSM and DM control loops closed both HLC and SPC are able to maintain their contrasts to better that 10^{-8} with the presence of WFIRST-like LoS variations (~14 mas drift and ~2 mas jitter) and slow varying low order WFE disturbances (~1 nm rms at ~1 mHz) (Shi et al. 2017). Although HabEx's LOWFS architecture is traceable to that of the WFIRST CGI, this LOWFS technology will have to be demonstrated in conjunction with the HabEx nominal VVC.

3.11 Deformable Mirrors

The baseline DMs are 64-actuator by 64-actuator by Boston Micromachines Corporation (BMC). The DMs are microelectromechanical systems (MEMS) made using semiconductor device fabrication technologies. The DM has a continuous facesheet for the surface of the mirror; the actuators pull on the back of the mirror using capacitance with an electrode in the back plane. The 4,096-actuator DM has been used in ground based coronagraphy on the Gemini Planet Imager(Macintosh et al. 2014). The 4,096 DM has a 3.5 μm stroke and 400 μm pitch.

The current BMC DMs are undergoing modifications to improve performance. Recent advances have reduced facesheet quilting to 3.3 nm rms. Facesheet scalloping is also being reduced by using a lower operating voltage. The best flattened WFE achieved in air to date is measured at about 6 nm rms. Additionally, the fabrication process of the DM has difficulty achieving 100% actuator yield. These challenges are currently being improved through a NASA Small Business Innovation Research (SBIR) program.

BMC DMs have proven useful for ground-based coronagraph instruments and have flown suborbital in a sounding rocket. Additional use of the BMC DMs is underway in more ground-based instruments, a high precision testbed, and in space on a CubeSat (**Table 3**).

A TDEM is currently underway to put 16 BMC DMs through environmental testing with pre-test and post-test performance characterization (Bierden 2013). Environmental testing of the BMC DMs as part of the TDEM is scheduled for 2018. The deepest raw contrast achieved by a coronagraph using the BMC DM was 2×10^{-7} over 2–11 λ/D at 650 nm

central wavelength and 10% bandwidth in the EXCEDE proposal testbed (Sirbu et al. 2016). Further coronagraph testing with BMC DMs will be carried out in the ExEP Decadal Survey Testbed starting this year. Should the new coronagraph tests achieve a 1×10^{-10} raw contrast under simulated environmental disturbances then the coronagraph and the BMC DMs will be at TRL 5.

Table 3. Boston Micromachines Corporation DMs in current and planned astronomical use.

Environment	Actuators	Instrument	Location
Ground	140	ROBO-AO	Palomar 2012, Kitt Peak 2015
Ground	1,024	Shane-AO	Lick Observatory 2013
Ground	2,040	SCExAO	Subaru 2013
Ground	4,092	GPI	Gemini South 2013
Space	1,024	PICTURE-B	Sounding Rocket 2015
Ground	2,040	MagAO-X	U of Az, *In work*
Ground	492	Rapid Transit Surveyor	U of H, *In work*
Ground	*952*	Keck Planet Imager and Characterizer	Keck, *In work*
Testbed	1,000 segments	Caltech HCST	Testbed, *In work*
Space	140	DEMI	CubeSat, *In work*

3.12 Starshade Edge Scatter Suppression

The primary goal of the starshade optical edges is to provide the correct apodization function needed to suppress starlight to levels suitable for exoplanet direct imaging. To do this, light emanating from other sources—principally petal edge-scattered sunlight—must be addressed since this scattered light can significantly degrade image contrast. The intensity of this scattered light must be limited to below the exozodiacal background.

Light scatter is driven by both the area and reflectivity of the scattering surface. As such, to mitigate edge-scatter, the starshade optical edges must have a sharp, beveled edge, and a surface with low reflectivity. Achieving these two edge characteristics has been the focus of edge-scatter technology work since 2015.

To resolve this technology gap, two parallel development efforts were initiated: a JPL effort focused heavily on creating sharp edges, and a Northrop Grumman Aerospace Systems (NGAS) effort centered on low reflectance. In 2015, JPL funded an effort to produce prototype optical edges. These edges were constructed using thin strips of amorphous metal as the absence of material grain structure allows for extremely sharp edges. Chemical etching techniques were used to manufacture the edges as it provides a means to produce the necessary beveled edge and can be implemented on meter-scale edge segments with micron-level in-plane tolerances. Multiple coupon samples were constructed and their geometry characterized using scanning electron microscope (SEM) images (**Figure 10**). A terminal radius of <0.5 μm was achieved with low levels of variability across each coupon. The solar glint performance of these coupons was also established using a custom scattered-light testbed; measurements indicate that the scattered flux is dimmer than the predicted intensity of the background zodiacal light over a broad range of sun angles. Further improvements to this performance can be achieved through the addition of low-reflectivity coatings on the optical edge—an area currently in development. While suitable solar glint performance was demonstrated at the coupon level, meter-scale development is still underway. Demonstration at the edge segment level—and accordingly, achievement of TRL-5—is expected by FY2020 through the S5 task (Ziemer 2018).

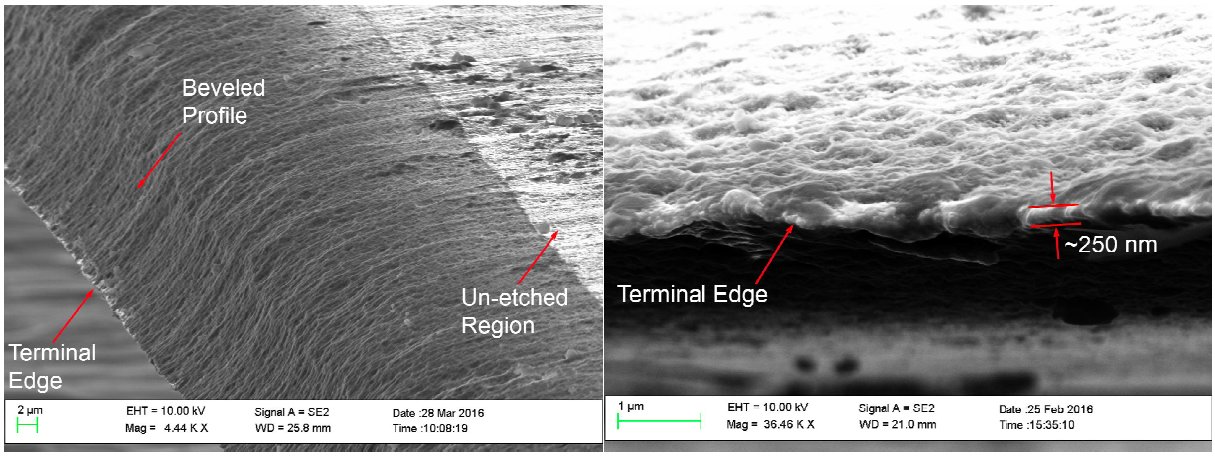

Figure 10. SEM images of the beveled edge and terminal edge

4. TECHNOLOGIES AT TRL 5 OR HIGHER

Some of the technologies in the HabEx design are anticipated to be at TRL 5 or higher by the release of the HabEx final report, including: microthrusters, deformable mirrors, low-noise visible and UV detectors, starshade formation flying, and laser metrology. This section describes the SOA of these technologies and how the SOA is applied to the HabEx design.

4.1 Starshade Starlight Suppression and Model Validation

As noted earlier, system-level performance testing of a flight-like starshade (contrast and IWA validation) is not possible on the ground due to the separation distance (124,000 km) required between the telescope and the occulter. Validation must be done through models and reduced-scale testing. To achieve the required image contrast, the two key model parameters are the Fresnel number and the ratio of the radius of the starshade's shadow at the telescope aperture, to the starshade's radius. The Fresnel number is defined as

$$F = \frac{r^2}{\lambda L}$$

Where r is the starshade radius, L is the starshade/telescope separation distance, and λ is the wavelength of the light being measured.

For HabEx, the Fresnel number is 10.45 (at λ = 1 µm) and the aperture-shadow-to-starshade ratio is 0.083. Any systems sharing these values will have the same contrast performance regardless of the occulter size and system separation distance. This model behavior allows ground testing of scaled-down versions of the starshade direct imaging system, to assess the optical performance of the flight system.

Such scaled testing is already underway through the S5 project. A testbed has been built at Princeton University (**Figure 11**) for starshade optical performance testing and model verification. The testbed illuminates the starshade mask with a 633 nm laser. Contrast levels are detected with an electron multiplying charge coupled device (EMCCD) observing the 50 mm starshade through a 4-mm aperture. The starshade and aperture are separated by 50 m. The deepest starshade model suppression achieved so far has been $1\times10^{-7.5}$ suppression at Fresnel number of 14.5 with a corresponding image plane contrast of 1×10^{-9} (Kim et al. 2017). The expectation is to achieve $<1\times10^{-10}$ contrast and TRL 5 in 2018 (Ziemer 2018).

Figure 11. S5's starshade model validation testbed at Princeton. Model starshade shown in inset.

4.2 Starshade Lateral Formation Sensing

Technology work on formation flying is also addressed through the S5 technology development task. S5 will fully address the HabEx formation flying gap and bring the technology to TRL 5 this year. Specifically, S5 will demonstrate lateral sensing of the starshade to less than 0.2 m, and control to within 1 m radial.

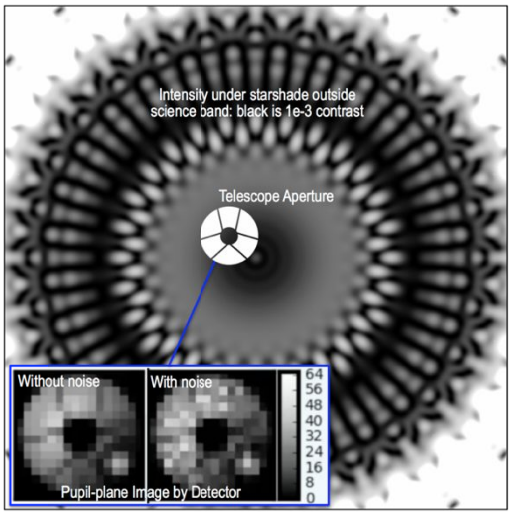

Figure 12. Illustration of approach for precision lateral sensing using pupil-plane image matching.

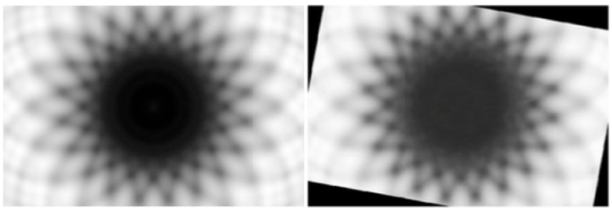

Figure 13. Preliminary results from the Low Contrast Testbed. *Left:* Simulated image. *Right:* Testbed image.

The sensing approach uses pupil-plane images at a wavelength outside the science band, where the starshade's attenuation of the starlight is only ~10^{-4} (see **Figure 12**). The shadow has sufficient structure at the center, that matching de-trended pupil-plane images to a library of pre-generated images can determine lateral position of the starshade to 15 cm (3σ) with short exposures. See Section 5.8.4 for more details on the design and operation of the HabEx formation flying system.

By the end of FY18, S5 will have demonstrated this sensing approach in a scaled 2 m low contrast testbed operating at a realistic Fresnel number with a 6 mm starshade, and with the detector mounted on a motion stage(Bottom 2017). The detector will be placed at a number of positions including corner cases (position extrema), and the output of the sensing

algorithm will be recorded. By comparing the sensor output and the truth positions from the motion stage, the predicted accuracies and precisions of the sensing approach will be verified to TRL 5. An example comparison of a predicted image and an initial image from the low contrast testbed is shown in **Figure 13**.

Following closure of the sensing gap, formation control will be demonstrated in simulation using a noise model for the lateral sensor. The noise model will have been verified during the earlier formation sensing work. The control simulation will include realistic thruster dynamics that require thrust allocation, thruster minimum impulse, and errors in attitude knowledge of the starshade. The dynamics will use a representative maximum gravity gradient and the control will be done with an optimal circular deadbanding algorithm, including representative drift times between thruster firings. In addition, an estimator combining the lateral sensor and radio frequency (RF) ranging measurements will be developed. Realistic actuator misalignments and mass property uncertainties will also be included. Work will be completed, and the HabEx formation flying technology will be at TRL 5 by the end of calendar 2018 (Ziemer 2018).

4.3 Microthrusters

Colloidal microthrusters (CMTs) provide low-noise, precise thrust and drag-free operation of spacecraft against disturbances—mainly solar pressure—for ultra-fine pointing and telescope stability control. Busek Co., Inc. has worked with JPL to provide two clusters of 4 CMTs (**Figure 14**) for the NASA Space Technology 7 Disturbance Reduction System (ST7-DRS) mission in 2008. ST7-DRS was launched on board the European Space Agency's (ESA's) LISA Pathfinder (LPF) Spacecraft in December 2016, and accumulated over 100 days of operation on orbit. The LPF CTMs were single string designs, intended for only 90 days of operation. Each thruster emits a finely controlled electrospray (electrostatically accelerated charged droplets) using an ionic liquid propellant, producing between 5–30 μN of thrust with 100 nN resolution All eight thrusters demonstrated full thrust range and controllability after 8 years of ground storage. As a system, thrust noise has been measured using ESA's inertial sensor on the LISA Technology Package (LTP) at levels ≤0.1 μN/√Hz (average per thruster.

Figure 14. A single cluster of four Busek Co. CMTs integrated on the LISA Pathfinder Spacecraft just prior to launch. Image courtesy ESA / Airbus.

NASA's Physics of the Cosmos (PCOS) Program is currently developing the colloidal microthruster technology as a potential contribution to the ESA-led LISA mission. During the next three years, the CMTs will be redesigned to be fully redundant with sufficient capacity to support a 12-year mission. Minor changes over the ST7's TRL 7 design are expected to be needed to meet lifetime and redundancy requirements; the redesigned thrusters are expected to reach TRL 6 at the end of the PCOS technology program. For HabEx, the reliability and lifetime technology development activities for LISA would provide a strong basis for CMT use. Studies are currently ongoing to determine thrust range requirements and propellant-minimizing thruster configurations for HabEx.

HabEx is also continuing to consider the Gaia cold-gas microthrusters as an alternative. The Gaia thrusters will have been operational at L2 for 5 years when the HabEx final report is delivered so they will have reached the HabEx

baseline lifetime requirement. However, their specific impulse is lower than the CTMs so more fuel would be required. While HabEx is baselining the CTMs for the interim report, the final decision on microthrusters will come after the report release.

4.4 Laser Metrology

A laser metrology truss provides the sensing end of a Laser Metrology Subsystem (MET) rigid body control loop for the HabEx telescope optics. Using rigid body actuators on the secondary and tertiary mirrors, MET actively maintains alignment of the front-end optics, removing the primary source of telescope wavefront drift. This breakthrough technology operates at high bandwidth and can maintain control throughout all phases of the mission, effectively creating a near perfect, infinitely stiff, telescope truss.

The backbone of MET is the laser metrology gauge which monitors any changes in the distance to a retroreflector. Each planar lightwave circuit (PLC) beam launcher, or gauge, requires a stable laser source and a phase meter to operate. Each of these components are at TRL 6 or higher.

The laser source for MET at JPL has historically been a Nd:YAG non-planar ring oscillator (NPRO). A similar, TRL 9, Nd:YAG ring laser has flown on LISA Pathfinder for the laser metrology system monitoring the test masses (Voland et al. 2017). Since laser metrology operates as a heterodyne system, a thermally stabilized PLC beam launcher (**Figure 15**) is sufficient for the purposes of HabEx.

The phase meter monitors the heterodyne measurement signal and compares it to the reference signal. Changes in the phase between the two signals are directly related to the change in the distance between the PLC beam launcher and the retroreflector. The LISA Pathfinder phase meter is an example of a suitable phase meter that is at TRL 9.

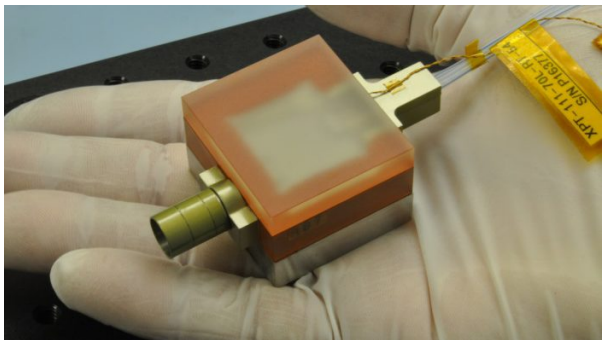

Figure 15. PLC beam launcher.

The final component of the MET system is the beam launcher. For HabEx, the beam launcher is the beam splitting/combining system that must be mounted to the telescope optics and therefore must be small and of similar construction. The PLC beam launcher evolved from the large, external metrology beam launchers developed for the Space Interferometry Mission and has been refined into a very compact, stable component. Continued development at JPL beyond the cancellation of the Space Interferometry Mission (SIM) in 2010 has brought these beam launchers up to TRL 6.

4.5 Detectors

HabEx can achieve its primary exoplanet scientific objectives with detectors that operate within the 300–1,000 nm spectral range. High performance in this range can be achieved using existing silicon-based detectors (e.g., CCDs and CMOS, arrays) with high TRL. Extending the spectral range at both ends enables a greater return for the exoplanet science and is required to meet general astrophysics and solar system science. This extended spectral coverage necessitates a closer look at existing detector capabilities in the UV down to 115 nm and in the NIR out to about 1,800 nm.

This section introduces detector candidates that have been selected by careful examination of the performance and latest status of the available technologies. The principles of operation for these detectors are briefly described and information is provided on the performance of their major relevant parameters, TRL status, and the path of further development.

4.6 Delta-Doped Visible EMCCDs

Electron multiplying charge-coupled devices are otherwise conventional CCDs that possess high S/N by the virtue of having an additional serial register. This so-called 'gain' register produces gain via avalanche multiplication in a stochastic process. Gains of greater than 1,000 can be achieved and photon counting can be performed. The Teledyne e2v's CCD 201, which has been baselined for the WFIRST coronagraph, has also been optimized for high efficiency and high stability in the 400–1,000 nm range using delta doping processes.

Extensive radiation testing for WFIRST has been carried out as part of the WFIRST CGI technology development program. The CCD201 is currently at TRL 5 for WFIRST, which has a nearly identical environment as HabEx(Harding et al. 2015).. Recent simulations informed by these results show that, although traps are formed in the radiation environment, the EMCCD still meets the WFIRST requirements. WFIRST CGI is incorporating an industry standard overspill drain to mitigate cosmic rays, as well as narrower pixel channels to help maintain Charge Transfer Efficiency in the presence of traps (Harding 2018). A larger format EMCCD (4k × 8k, CCD282) by Teledyne-e2v is baselined for HabEx. Recent results show improved performance in 4kx4k in terms of cosmic rays by incorporation of overspill drain in CCD282 (Daigle 2018).

4.7 Linear Mode Avalanche Photodiode Near-IR Detectors

Leonardo-ES Ltd in Southampton, UK, has been developing HgCdTe avalanche photo diode (APD) sensors for astronomy in collaboration with the European Southern Observatory and the University of Hawaii since 2008. The devices use metalorganic vapor phase epitaxy (MOVPE) grown on gallium arsenide (GaAs) substrates. This, in combination with a mesa device structure, produces a detector that achieves a noiseless avalanche gain, very low dark current (due to band gap engineering) and a near-ideal spatial frequency response. A device identified as "Saphira"—a 320×256, 24 μm pixel detector—has been developed for wavefront sensors, interferometry, and transient event imaging and is currently in use in a number of ground-based telescopes including Subaru and NASA's Infrared Telescope Facility.

Saphira has demonstrated read noise as low as 0.26 electrons rms and single photon imaging with avalanche gains of up to 500. An avalanche gain of 5 can be achieved with dark current of less than 0.002 electrons per second per pixel. This dark current translates into nearly a factor of five improvement in S/N for signals of the order of 100 photons, or a factor of 25 improvement in observation time. The Saphira detectors have been assessed at TRL 5, which means they have been tested in a relevant environment. There is a current ESA program to assess radiation (gamma and proton) resilience and, to date, there has been no change in the detector performance after exposures of 50 krads of gamma radiation. Two devices were exposed to total ionizing doses of ~30 and 50 krads (simulating long term exposure): no significant degradation of the performance was observed during or after the exposure. Four devices were exposed to proton irradiation, two at 100 K and two at ambient temperature: no variation in the avalanche process was observed in the intermediate measurements, and additionally there was no long term degradation of the dark current (measured after a few weeks at room temperature).

Currently, there is a NASA program funding development of a custom MOVPE design for low-background/high-gain imaging aimed at extending the gain and reducing dark current of the Saphira detectors even further.

4.8 UV Microchannel Plate Detectors

Microchannel plates (MCPs) have been the workhorse of ultraviolet instruments for several decades. They are image tube–based detector technologies in which a photocathode material is used to absorb photons in the desired spectral range, creating electrons that are accelerated in vacuum and multiplied in the tube. The gain achieved in this fashion and the low background noise renders MCPs highly applicable in photon-counting applications. The charge packet exiting the MCP tubes is detected through various readout schemes depending on the application.

Microchannel plate detectors have flown on UV astronomical missions (FUSE, GALEX, HST-COS). More recent MCP detector developments include atomic layer deposition (ALD) on borosilicate microcapillary arrays. An ALD MCP detector has flown on the LITES ISS instrument (Siegmund et al. 2017).

Continued development of UV MCP detectors will improve performance and packaging in the coming years. In 2012, a NASA Strategic Astrophysics Technology (SAT) grant was awarded to raise the TRL of a 50 mm square cross-strip MCP detector from 4 to 6. The team was also funded in 2016 with a follow-on SAT to scale this detector to a flight

qualified 100×100 mm format (Vallerga et al. 2016). Even larger formats (200×200 mm) are also being developed. MCP detectors currently baselined for HabEx are TRL 5.

4.9 Delta-Doped UV EMCCDs

Delta-doped UV EMCCDs offer an alternative to current MCPs in the 100–300 nm wavelength range. High efficiency (>60% quantum efficiency) in the 100–400 nm range has also been demonstrated on EMCCDs. JPL has been working closely with e2v to develop the end-to-end processing for CCD 201 and has focused on the high efficiency and photon-counting performance of the detector. A delta-doped EMCCD with coatings to optimize the performance at 205 nm has been delivered to FIREBall, a balloon-based UV experiment, which is expected to launch this year. Another EMCCD that is optimized for 120–150 nm range is baselined on the sounding rocket SHIELDS, which is expected to fly in early 2019 advancing to TRL 6.

The delta-doping utilizes JPL's low temperature (<450°C) molecular beam epitaxy (MBE) growth process to inject dopant atoms in a highly localized layer. "Delta-doping creates very high electric fields near the surface that drive photogenerated charge away from the back surface and suppress the generation of excess dark current from the exposed silicon surface" (Hoenk et al. 2009).

5. TIMELINE FOR MATURITY

The S5 project and Decadal Studies Testbed bring to TRL 5 most of the needed technologies by end of FY 2022. A HabEx specific Coronagraph Instrument testbed could mature at Instrument level the coronagraph technologies (DM, LOWFS, coronagraph architecture) to TRL 5 by 2022. If HabEx were to be prioritized by the Decadal Review Committee; then HabEx specific technology development is estimated to start with FY 2022. The potential starshade petal deployment activities could reach TRL 5 in 2025, or in 2021 if the final starshade design is close enough in scale to the S5 test piece. The HabEx primary mirror prototype and coating if started in FY 2022 could finish at the end of FY 2026.All HabEx technology challenges could reach TRL5 by 2026.

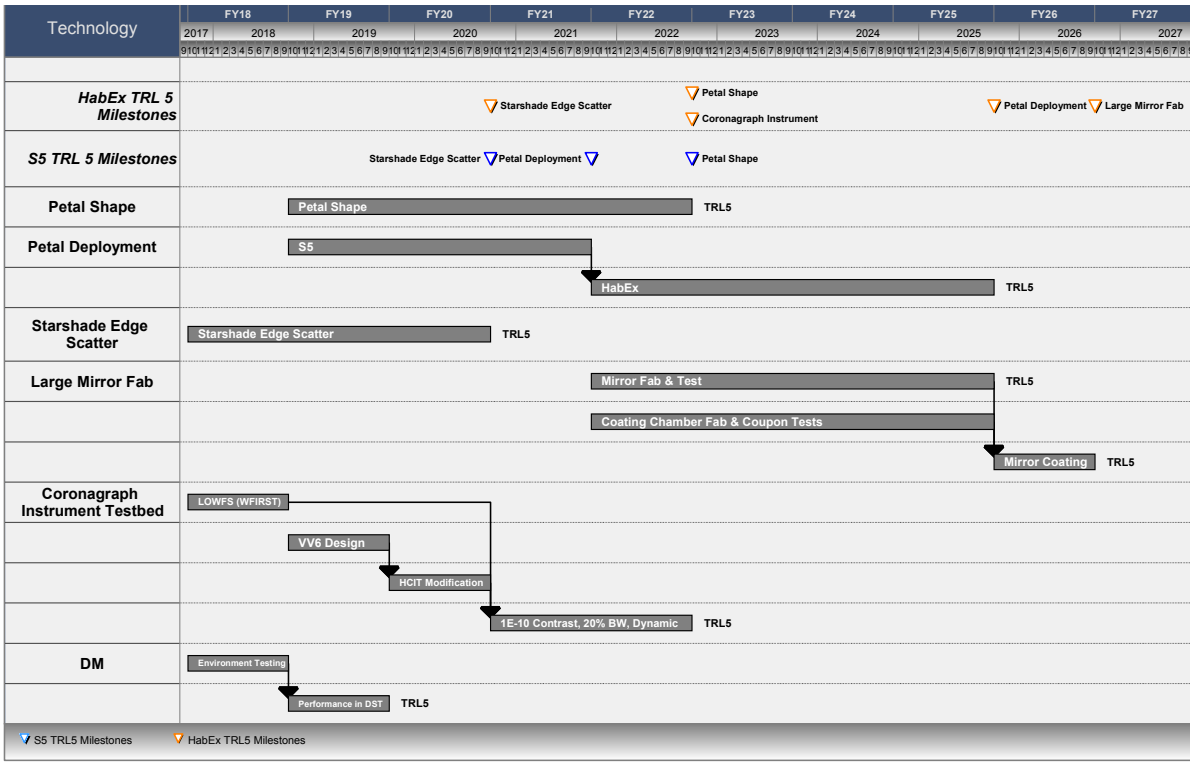

Figure 16. The timeline for technology development shows S5 TRL 5 milestones as well as HabEx specific activities. All HabEx technology challenges could reach TRL5 by 2026.

ACKNOWLEDGEMENTS

The HabEx Concept design is pre-decisional information presented for planning and discussion purposes only. This work was carried out at the Jet Propulsion Laboratory, California Institute of Technology, under contract with the National Aeronautics and Space Administration.

REFERENCES

[1] Balasubramanian, Kunjithapatham, John Hennessy, Nasrat Raouf, Shouleh Nikzad, Michael Ayala, Stuart Shaklan, Paul Scowen, Javier Del Hoyo, and Manuel Quijada. 2015. "Aluminum mirror coatings for UVOIR telescope optics including the far UV." UV/Optical/IR Space Telescopes and Instruments: Innovative Technologies and Concepts VII.

[2] Balasubramanian, Kunjithapatham, John Hennessy, Nasrat Raouf, Shouleh Nikzad, Javier Del Hoyo, Manuel Quijada. 2017. "Mirror coatings for large aperture UV optical infrared telescope optics," UV/Optical/IR Space Telescopes and Instruments: Innovative Technologies and Concepts VIII

[3] Bierden, Paul. 2013. TDEM Awards. NASA Exoplanet Exploration Program Accessed December 9.

[4] Blackwood, G., Seager, S., Siegler, N., Noecker, C., Hyde, T. 2016. Starshade Readiness Working Group Recommendation to Astrophysics Division Director. Starshade Readiness Working Group. Accessed November 9.

[5] Bottom, Michael, Stefan Martin, Carl Seubert, Eric Cady, Shannon Kian Zareh, Stuart Shaklan, "Precise starshade stationkeeping and pointing with a Zernike wavefront sensor," Proc. SPIE 10400, Techniques and Instrumentation for Detection of Exoplanets VIII, 104001B (1 September 2017);

[6] Brooks, Thomas E., Ron Eng, Tony Hull, H. Philip Stahl. 2017. "Modeling the Extremely Lightweight Zerodur Mirror (ELZM) thermal soak test," Optical Modeling and Performance Predictions IX

[7] Cohen, Eri Jay, and Tony Hull. 2004. "Selection of a mirror technology for the 1.8-m Terrestrial Planet Finder demonstrator mission." Optical Fabrication, Metrology, and Material Advancements for Telescopes.

[8] Daigle, Olivier, Jeremy Turcotte, Etienne Artigau, Rene´ Doyon. 2018. "Preliminary characterization results of a larege format 4k x 4k EMCCD." High Energy, Optical and Infrared Detectors for Astronomy VIII,

[9] Fleming, B., M. Quijada, J. Hennessy, A. Egan, J. Del Hoyo, B. A. Hicks, J. Wiley, N. Kruczek, N. Erickson, and K. France, "Advanced environmentally resistant lithium fluoride mirror coatings for the next generation of broadband space observatories," Appl. Opt. 56 (36), 9941-9950 (2017).

[10] Harding, Leon K., Richard Demers, Michael E. Hoenk, Pavani Peddada, Bijan Nemati, Michael Cherng, Darren Michaels, Leo S. Neat, Anthony Loc, Nathan L. Bush, David J. Hall, Neil J. Murray, Jason P. D. Gow, Ross Burgon, Andrew D. Holland, Alice L. Reinheimer, Paul R. Jorden, Douglas Jordan. 2015. "Technology advancement of the CCD201-20 EMCCD for the WFIRST coronagraph instrument: sensor characterization and radiation damage," J. Astron. Telesc. Instrum. Syst. 2(1) 011007

[11] Harding, Leon K. 2018. "Deploying electron multiplying CCDs in photon starved coronagraph and spectrograph instruments for WFIRST (Conference Presentation)," Micro- and Nanotechnology Sensors, Systems, and Applications X,

[12] Hoenk, Michael E, Todd J Jones, Matthew R Dickie, Frank Greer, Thomas J Cunningham, Edward R Blazejewski, and Shouleh Nikzad. 2009. "Delta-doped back-illuminated CMOS imaging arrays: progress and prospects." Infrared Systems and Photoelectronic Technology IV.

[13] Hull, Tony, Thomas Westerhoff, Antoine Lays, and John Pepi. 2013. "Practical aspects of specification of extreme lightweight Zerodur mirrors for spaceborne missions." Optomechanical Engineering 2013.

[14] Jedamzik, Ralf, and Thomas Westerhoff. 2017. "Homogeneity of the coefficient of linear thermal expansion of ZERODUR: a review of a decade of evaluations." Astronomical Optics: Design, Manufacture, and Test of Space and Ground Systems.

[15] Kim, Yunjong, Anthony Harness, Dan Sirbu, Mengya Hu, Mike Galvin, N Jeremy Kasdin, Robert J Vanderbei, and Stuart B Shaklan. 2017. "Optical demonstration of a starshade at flight fresnel numbers." Techniques and Instrumentation for Detection of Exoplanets VIII.

[16] Lightsey, Paul A, Benjamin B Gallagher, Neal Nickles, and Tracy Copp. 2012. "Optical transmission for the James Webb Space Telescope." Space Telescopes and Instrumentation 2012: Optical, Infrared, and Millimeter Wave.

[17] Macintosh, Bruce, James R. Graham, Patrick Ingraham, Quinn Konopacky, Christian Marois, Marshall Perrin, Lisa Poyneer, Brian Bauman, Travis Barman, Adam S. Burrows, Andrew Cardwell, Jeffrey Chilcote, Robert J. De Rosa, Daren Dillon, Rene Doyon, Jennifer Dunn, Darren Erikson, Michael P. Fitzgerald, Donald Gavel, Stephen Goodsell, Markus Hartung, Pascale Hibon, Paul Kalas, James Larkin, Jerome Maire, Franck Marchis, Mark S. Marley, James McBride, Max Millar-Blanchaer, Katie Morzinski, Andrew Norton, B. R. Oppenheimer, David Palmer, Jennifer Patience, Laurent Pueyo, Fredrik Rantakyro, Naru Sadakuni, Leslie Saddlemyer, Dmitry Savransky, Andrew Serio, Remi Soummer, Anand Sivaramakrishnan, Inseok Song, S andrine Thomas, J. Kent Wallace, Sloane Wiktorowicz, Schuyler Wolff. 2014. "First light of the Gemini Planet Imager." Proceedings of the National Academy of Sciences Sep 2014, 111 (35) 12661-12666

[18] Oh, Chang Jin, Andrew E. Lowman, Greg A. Smith, Peng Su, Run Huang, Tianquan Su, Daewook Kim, Chunyu Zhao, Ping Zhou, James H. Burge. 2016. "Fabrication and testing of 4.2m off-axis aspheric primary mirror of Daniel K. Inouye Solar Telescope," Proc. SPIE 9912, Advances in Optical and Mechanical Technologies for Telescopes and Instrumentation II

[19] Pham, Bruce Thai, and Susan Gale Neff. 2016. "Cosmic Origins Program Annual Technology Report."

[20] Seager, Sara, W Cash, S Domagal-Goldman, NJ Kasdin, M Kuchner, A Roberge, S Shaklan, W Sparks, M Thomson, and M Turnbull. 2015. "Exo-S: starshade probe-class exoplanet direct imaging mission concept final report." available at exep. jpl. nasa. gov/stdt.

[21] Serabyn, E, J Trauger, D Moody, D Mawet, K Liewer, J Krist, and B Kern. 2013. "High-contrast imaging results with the vortex coronagraph." Techniques and Instrumentation for Detection of Exoplanets VI.

[22] Shaklan, Stuart B, Luis Marchen, and Eric Cady. 2017. "Shape accuracy requirements on starshades for large and small apertures." Techniques and Instrumentation for Detection of Exoplanets VIII.

[23] Sheikh, DA, SJ Connell, and RS Dummer. 2008. "Durable silver coating for Kepler Space Telescope primary mirror." Space Telescopes and Instrumentation 2008: Optical, Infrared, and Millimeter.

[24] Shi, Fang, Eric Cady, Byoung-Joon Seo, Xin An, Kunjithapatham Balasubramanian, Brian Kern, Raymond Lam, David Marx, Dwight Moody, and Camilo Mejia Prada. 2017. "Dynamic testbed demonstration of WFIRST coronagraph low order wavefront sensing and control (LOWFS/C)." Techniques and Instrumentation for Detection of Exoplanets VIII.

[25] Siegmund, OHW, C Ertley, JV Vallerga, ER Schindhelm, A Harwit, BT Fleming, KC France, JC Green, Stephan R McCandliss, and WM Harris. 2017. "Microchannel plate detector technology potential for LUVOIR and HabEx." UV, X-Ray, and Gamma-Ray Space Instrumentation for Astronomy XX.

[26] Sirbu, Dan, Sandrine J Thomas, Ruslan Belikov, Julien Lozi, Eduardo A Bendek, Eugene A Pluzhnik, Dana H Lynch, Troy T Hix, Peter T Zell, and Olivier Guyon. 2016. "Demonstration of broadband contrast at 1.2 λ/D and greater for the EXCEDE starlight suppression system." Journal of Astronomical Telescopes, Instruments, and Systems 2 (2):025002.

[27] Trauger, John, Brian Gordon, John Krist, and Dwight Moody. 2015. "Hybrid Lyot coronagraph for WFIRST-AFTA: coronagraph design and performance metrics." Techniques and Instrumentation for Detection of Exoplanets VII.

[28] Vallerga, John, Jason McPhate, Anton Tremsin, Oswald Siegmund, Rick Raffanti, Harley Cumming, Andrej Seljak, Vihtori Virta, and Gary Varner. 2016. "Development of a flight qualified 100 x 100 mm MCP UV detector using advanced cross strip anodes and associated ASIC electronics." Space Telescopes and Instrumentation 2016: Ultraviolet to Gamma Ray.

[29] Voland, C, G Lund, W Coppoolse, P Crosby, M Stadler, K Kudielka, and C Özkan. 2017. "Laser modulator for lisa pathfinder." International Conference on Space Optics—ICSO 2008.

[30] Wang, Xu, J. Kent Wallace, Fang Shi. (2015) "Zernike wavefront sensor modeling development for LOWFS on WFIRST-AFTA." Techniques and Instrumentation for Detection of Exoplanets VII

[31] Westerhoff, Thomas, and Thomas Werner. 2017. "ZERODUR expanding capabilities and capacity for future spaceborne and ground-based telescopes." Astronomical Optics: Design, Manufacture, and Test of Space and Ground Systems.

[32] Ziemer, J., Lisman, D., Martin, S., Shaklan, S., Webb, D., Warwick, S., Seager, S., Kasdin, J., Harness, A. 2018. White Paper on Starshade Technology Development: Preparing for an Exoplanet Observatory Mission in the Next Decade. NAS Exoplanet Science Strategy. Accessed March 12.